

Dynamically induced magnetism in KTaO_3 R. Matthias Geilhufe¹, Vladimir Juričić^{1,2}, Stefano Bonetti^{3,4}, Jian-Xin Zhu⁵, and Alexander V. Balatsky^{1,6}¹*Nordita, KTH Royal Institute of Technology and Stockholm University, Roslagstullsbacken 23, 10691 Stockholm, Sweden*²*Departamento de Física, Universidad Técnica Federico Santa María, Casilla 110, Valparaíso, Chile*³*Department of Physics, Stockholm University, 10691 Stockholm, Sweden*⁴*Department of Molecular Sciences and Nanosystems, Ca' Foscari University of Venice, 30172 Venice, Italy*⁵*Theoretical Division and Center for Integrated Nanotechnologies, Los Alamos National Laboratory, Los Alamos, New Mexico 87545, USA*⁶*Department of Physics and Institute for Materials Science, University of Connecticut, Storrs, Connecticut 06269, USA*

(Received 12 March 2021; revised 9 April 2021; accepted 14 April 2021; published 10 May 2021)

Dynamical multiferroicity features entangled dynamic orders: fluctuating electric dipoles induce magnetization. Hence, the material with paraelectric fluctuations can develop magnetic signatures if dynamically driven. We identify the paraelectric KTaO_3 (KTO) as a prime candidate for the observation of the dynamical multiferroicity. We show that when a KTO sample is exposed to a circularly polarized laser pulse, the dynamically induced ionic magnetic moments are of the order of 5% of the nuclear magneton per unit cell. We determine the phonon spectrum using *ab initio* methods, and we identify T_{1u} as relevant phonon modes that couple to the external field and induce magnetic polarization. We also predict a corresponding electron effect for the dynamically induced magnetic moment, which is enhanced by several orders of magnitude due to the significant mass difference between electron and ionic nucleus.

DOI: [10.1103/PhysRevResearch.3.L022011](https://doi.org/10.1103/PhysRevResearch.3.L022011)

Introduction. Dynamical multiferroicity [1], the phenomenon where fluctuating electrical dipoles induce magnetization, represents the dynamical counterpart of the Dzyaloshinskii-Moriya mechanism [2]. The origin of this effect lies in the duality between the electric and magnetic properties [3]. Quite generally, the effect features entangled quantum orders. Most notably, displacive paraelectrics (PE) exhibiting a ferroelectric (FE) phase transition [4–11] can display an elevated magnetic response induced by either quantum [12] or thermal fluctuations [13] close to the critical point. On the other hand, the dynamical magnetization can be induced by externally driving the material, e.g., by applying the light or a lattice strain [1]. Dynamic multiferroicity is an example of the nonlinear phononics phenomenology [14], where a two-phonon process induces magnetization. From the perspective of the materials where dynamical multiferroicity can be realized, the prime candidate to search for the effect is SrTiO_3 (STO), the paradigmatic quantum critical paraelectric where ferroelectricity is induced by displacive fluctuations. It has been recently predicted that the magnetization dynamically induced both by external means and intrinsically, close to the FE QCP in this material, may be in a measurable range [12,13].

In contrast to STO, KTaO_3 (KTO) is a quantum disordered paraelectric at low temperatures with a significantly gapped

transverse optical mode [5]. At zero stress, KTO retains its cubic structure down to helium temperatures [15]. The transition into a ferroelectric phase in KTO can be induced as well, e.g., by impurities [16,17] or strain [18]. It is assumed that the ground state of KTO is a quantum disordered phase and significantly away from quantum critical fluctuations. Since KTO behaves as a regular quantum paraelectric, quantum critical modes are gapped. Furthermore, on the paraelectric side of the quantum critical point, the fluctuations of the polarization are expected to be stronger and might give rise to a more dominant signal of a dynamically induced magnetic moment. So far, no prediction regarding the effect of dynamically induced magnetization has been made for KTO, and this is precisely the aim of the current paper.

Following the formalism of dynamical multiferroicity [1,12,13], we investigate the induction of magnetic moments by applying circularly polarized terahertz radiation resonant with the phonon frequency that yields fluctuating local electric dipoles, according to

$$\mathbf{M} = \alpha \mathbf{P} \times \frac{\partial}{\partial t} \mathbf{P} = \gamma \mathbf{u} \times m \frac{\partial}{\partial t} \mathbf{u}. \quad (1)$$

Here, \mathbf{M} denotes the local magnetic moment, \mathbf{P} the electric polarization, \mathbf{u} the atomic displacement (associated with the relevant phonon mode in our analysis), m the particle mass, while α and the gyromagnetic ratio γ are the respective coupling constants. By performing an *ab initio* analysis of the phonon spectrum (see Fig. 1), we single out T_{1u} IR active phonon modes as relevant for the dynamical multiferroicity. As we show, using both single-mode approximation and the full dynamical matrix approach, when the system is subjected to a resonant circularly polarized laser pulse (Fig. 2), one

Published by the American Physical Society under the terms of the Creative Commons Attribution 4.0 International license. Further distribution of this work must maintain attribution to the author(s) and the published article's title, journal citation, and DOI.

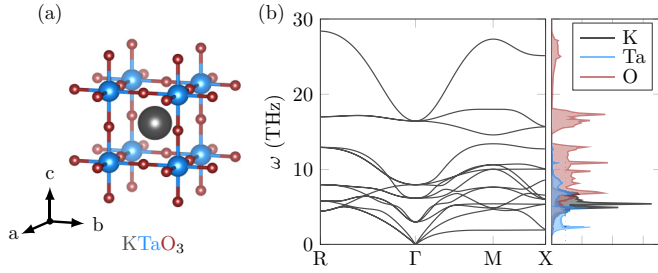


FIG. 1. (a) Unit cell of KTaO_3 . (b) Calculated phonon spectrum and phonon density of states.

obtains a measurable magnetic signal. Taking a realistic value of the damping for the mode, we find that the induced magnetic moment per unit cell can reach values of $\sim 0.05\mu_N$, where μ_N is the nuclear magneton. We also predict an enhancement of the effect due to the coupling of the ion dynamics with the electronic one, which should be detectable experimentally.

Phonon spectrum: First-principles calculation. KTO crystallizes in a cubic lattice with space group $Pm\bar{3}m$ [Fig. 1(a)]. We chose the experimental lattice constants as determined by Zhurova *et al.* [19], with a unit-cell volume of 63.44 \AA^3 . The phonon spectrum was calculated using PHONOPY [20]. The related force matrix was obtained from a $2 \times 2 \times 2$ supercell with automatically generated displacements, where forces were calculated using the Vienna *ab initio* simulation package VASP [21]. The exchange correlation functional was approximated by the PBE functional [22]. We chose $8 \times 8 \times 8$ points for the Brillouin zone integration, which corresponds to a \mathbf{k} -mesh density of $\approx 1050 \text{ k-points/\AA}^{-3}$. We used a cutoff energy of 700 eV. Additionally, we calculated the Hessian matrix for the energy landscape using density functional perturbation theory. This approach also provides a force matrix and phonon frequencies at the Γ point, which we used to estimate the dynamically induced magnetization, as explained below.

The KTO unit cell contains five inequivalent sites, resulting in 15 phonon modes. We studied the symmetry of the phonon modes using GTPACK [23,24]. Constructing a five-dimensional permutation representation Γ_p for the point group O_h and the five unit-cell sites and computing the direct product with the vector representation $\Gamma_v = T_{1u}$, we obtain $\Gamma_p \otimes \Gamma_v \approx$

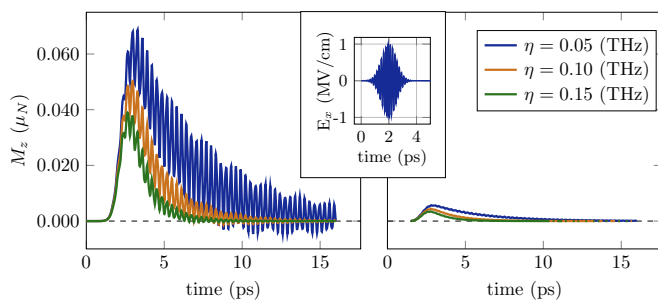


FIG. 2. Dynamically induced total moment per unit cell for a laser pulse with driving frequencies 3.05 THz (left panel) and 6.17 THz (right panel).

TABLE I. Calculated Born effective charges in units of the elementary charge e .

	Z_{xx}^*	Z_{yy}^*	Z_{zz}^*
K	1.14	1.14	1.14
O	-6.64	-1.68	-1.68
O	-1.68	-6.64	-1.68
O	-1.68	-1.68	-6.64
Ta	8.86	8.86	8.86

$4T_{1u} \oplus T_{2u}$ corresponding to the expected modes at the Γ -point in the Brillouin zone [24]. Using PHONOPY, we verify four T_{1u} modes at frequencies 0.0, 3.02, 6.16, and 16.38 THz, as well as one T_{2u} mode at 7.94 THz. The former modes being IR active but finite-frequency modes are instrumental for the dynamical multiferroicity, as shown below. The full phonon spectrum showing 3 acoustic and 12 optical modes is plotted in Fig. 1(b). The values are in good agreement with previous experiments on KTO [25]. These frequencies change slightly when calculated using the density functional perturbation theory, giving 0.0, 3.05, 6.17, 7.98, and 16.41 THz. We notice that, in contrast to STO, KTO does not give rise to negative energy modes in the phonon spectrum for the cubic phase, indicating the absence of a structural phase transition at low temperatures. After identifying the T_{1u} phonon modes, we analyze the magnetic signal resulting from the exposure of the KTO system to an externally applied circularly polarized laser pulse.

Dynamical multiferroicity. The polarization contains an ionic and an electronic contribution and can be written as

$$P_{i\alpha} = Z_{i\alpha\beta}^* u_{i\beta} + \epsilon_0(\epsilon_{\alpha\beta} - \delta_{\alpha\beta})E_{\beta}. \quad (2)$$

Here $u_{i\alpha}$ denotes a displacement of atom i along the Cartesian coordinate α . The Born effective charge $Z_{i\alpha\beta}^*$ describes the response of the macroscopic polarization per unit cell to the displacement of atom i , $Z_{i\alpha\beta}^* = \Omega \frac{\partial P_{\beta}}{\partial u_{i\alpha}}|_{\mathbf{E}=0}$, with Ω the unit-cell volume [26]. The calculated Born effective charges for KTO are given in Table I. The electronic response of the polarization to the electric field is approximated in terms of the static dielectric tensor ϵ_{ij} . Due to the cubic symmetry of the unit cell, the dielectric tensor is diagonal and we obtain

$$\epsilon_{xx} = \epsilon_{yy} = \epsilon_{zz} = 5.4. \quad (3)$$

This value is sensitive to the chosen computational parameters, but consistent with other references [27]. $\epsilon_0 \approx 5.52 e^2 \text{ keV}^{-1} \text{ \AA}^{-1}$ is the vacuum permittivity.

We calculate atomic displacements \mathbf{u}_i at the site i using classical equations of motion,

$$\ddot{u}_{i\alpha}(t) + \eta \dot{u}_{i\alpha}(t) + \sum_{j\beta} K_{i\alpha j\beta} u_{j\beta}(t) = \frac{Z_{i\alpha}}{m_i} E_{\alpha}^*(t). \quad (4)$$

Here, $Z_{i\alpha} = Z_i^0 + \sum_{\beta} Z_{i\alpha\beta}^* u_{i\beta}$, with Z_i^0 being the bare charge of the ion (see Table II). m_i is the mass of atom i , η is a damping factor, and \mathbf{K} is the dynamical matrix. The electric field within the medium \mathbf{E}^* is related to the vacuum electric field \mathbf{E} by

$$\mathbf{E}^* = \epsilon^{-1} \mathbf{E}. \quad (5)$$

TABLE II. Site parameters. Charge values according to DFT calculations performed in this study.

	K	Ta	O
charge [$e \approx 1,602 \times 10^{-19}$ C]	0.867	4.954	-1.940
mass [$u \approx 1,66 \times 10^{-27}$ kg]	39.1	180, 95	16.0

In experiments, an additional loss in the field strength has to be taken into account due the polarization process. In our approach, the electric field induces a collective displacement of the ionic positions by coupling to the charge. Note that we do not include higher-order corrections to the dielectric screening [28].

We continue by discussing the size of the dynamically induced magnetic moment using a simplified analytical model. The full set of coupled differential equations is solved numerically afterward. We start by solving Eq. (4) within a single-mode approximation by considering one relevant mode $\omega_i = 2\pi f_i$, corresponding to one relevant site,

$$\ddot{u}_\alpha(t) + \eta \dot{u}_\alpha(t) + \omega_i^2 u_\alpha(t) = \frac{q}{m} E_\alpha^*(t). \quad (6)$$

We choose circularly polarized light, i.e., $\mathbf{E}^*(t) = E_0^*(\sin(\omega t), \cos(\omega t), 0)$. In a coarse approximation, from (6), we notice that the displacement scales linearly with the applied field, $\mathbf{u} \approx \frac{q\mathbf{E}^*}{m\omega^2}$. For a harmonic displacement, we can estimate the corresponding time derivative as $\dot{\mathbf{u}} \approx \omega\mathbf{u}$. Using Eq. (1) and replacing the gyromagnetic ratio by $\gamma = \frac{q}{2m}$, we can estimate the asymptotic behavior for the dynamically induced magnetic moment by

$$M_z \sim \frac{q^3 \mathbf{E}^{*2}}{m^2 \omega^3}. \quad (7)$$

Hence, the effect increases quadratically in the field strength, but decreases with ω^{-3} in the driving frequency. The corresponding values for the charge q and the mass m for KTO are given in Table II. The charges calculated using DFT are close to the chemistry picture of an ionic crystal, with integer oxidation states O^{-2} , K^{+1} , and Ta^{+5} .

Equation (6) can be solved exactly. As we are solely interested in the contribution to the atomic displacement emerging due to exposure to an external laser field, we only keep the inhomogeneous part of the solution of Eq. (4) that can be written as

$$\mathbf{u}(t) = \frac{1}{\Delta_\omega^4 + 4\eta^2\omega^2} \begin{pmatrix} \Delta_\omega^2 & -2\eta\omega \\ 2\eta\omega & \Delta_\omega^2 \end{pmatrix} \frac{q}{m} \mathbf{E}^*, \quad (8)$$

with $\Delta_\omega^2 = \omega_i^2 - \omega^2$. Evaluating the polarization as $\mathbf{P} = \frac{q}{V}\mathbf{u}$, the ω -dependent part of Eq. (8) can be interpreted as the susceptibility χ by transforming it into the well-known expression $\mathbf{P} = \chi \epsilon_0 \mathbf{E}$. Hence, we obtain for the magnetization

$$M_z = \frac{q^3 \omega \mathbf{E}^{*2}}{2m^2(\eta^2\omega^2 + \Delta_\omega^4)}. \quad (9)$$

In the limit $\omega \gg \omega_i$, we obtain $\Delta_\omega^4 \approx \omega^4$. Neglecting the damping term $\eta^2\omega^2 \ll \omega^4$ gives a similar expression to Eq. (7).

System driven with a terahertz pulse. Next, we consider a more realistic terahertz pulse and solve Eq. (4) numerically.

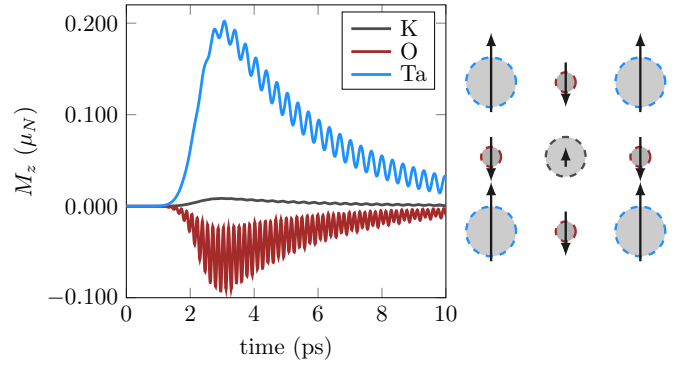


FIG. 3. Site-resolved dynamically induced moments within the unit cell. We used the same pulse as in Fig. 2, a driving frequency of 3.05 THz and a damping of $\eta = 0.05$ THz.

Such terahertz pulses are currently available [29] and allow for large peak electric field to drive phonons, but with an average deposited energy that is not enough to melt the sample. We set $\mathbf{u}_\alpha(0) = \dot{\mathbf{u}}_\alpha(0) = 0$. The pulse is modeled by a Gaussian embedding as follows:

$$\mathbf{E}(t) = E_0 e^{-\frac{(t-t_0)^2}{2\sigma}} \begin{pmatrix} \sin(\omega t) \\ \cos(\omega t) \\ 0 \end{pmatrix}. \quad (10)$$

The considered driving frequencies are 3.05 and 6.17 THz, being resonant with the phonon modes. We choose a total width of 2 ps with a peak at 2 ps and obtain the solution for a window up to 16 ps. The dynamically induced magnetic moments are shown in Fig. 2 for various values of the damping parameter ($\eta = 0.05, 0.10$, and 0.15 THz). Depending on the damping factor, we observe a slow decay of the dynamically induced magnetic moment. The maximal total dynamically induced magnetic moment is $\approx 0.7\mu_N$ for small damping of $\eta < 0.1$ THz. The dynamically induced magnetic moment decreases by about one order of magnitude for a driving frequency in resonance with the T_{1u} mode at 6.17 THz. Due to the opposite local charges of the ions, the induced moments have opposite strength for O compared to Ta and K. The site-resolved dynamically induced moments due to local displacements are shown in Fig. 3. We observe that the main contributions to the total induced magnetization per unit cell come from Ta and O, being of the order of $0.2\mu_N$ and $-0.1\mu_N$ for a small value of the damping parameter, $\eta = 0.05$ THz.

Conclusion and outlook. We showed that KTO is a prominent candidate for the observation of dynamical multiferroicity. We suggest an experimental setup where the KTO sample is exposed to a circularly polarized laser field in the terahertz range to excite phonons resonantly. Using *ab initio* calculations, we identify the T_{1u} phonon modes that couple to the laser pulse. The dynamically induced magnetization due to locally oscillating dipoles could be measured by the time-resolved Faraday effect using a femtosecond laser pulse in the visible range. The estimated scale of the effect for an experimentally feasible setup is in the order of $10^{-2}\mu_N$ per unit cell, with μ_N being the nuclear magneton. In Eq. (7) we show that in an asymptotic limit, the induced moment scales quadratically with the electric field strength and to the third power in the charge. It also scales inversely with the third

power in driving frequency and the mass squared. In particular the latter feature could be of interest.

Here we discussed the ionic movement as a driver for the induced magnetism. We now point out an interesting possibility of induced electron motion that also would produce the magnetic moment. We expect the angular momentum transfer from the moving ions to the electronic charge cloud in the solid. While the exact microscopic details need to be worked out, the qualitative argument goes as follows. To estimate the gyromagnetic ratio for the coupling, we follow Refs. [13,30] in a modified form. The position of a charged ion is denoted by \mathbf{u}_+ , and the average displacement of the electron cloud is \mathbf{u}_- . The respective masses are m_+ and m_- . We introduce average and relative coordinates $\mathbf{U} = (m_+\mathbf{u}_+ + m_-\mathbf{u}_-)/(m_+ + m_-)$ and $\mathbf{u} = \mathbf{u}_+ - \mathbf{u}_-$. We focus on the relative coordinate, having the momentum $\mathbf{p} = \mu\dot{\mathbf{u}}$ with $\mu = m_+m_-/(m_+ + m_-)$. It follows for the angular momentum of the relative coordinate

$$\mathbf{L} = \mathbf{u} \times \mathbf{p} = \frac{m_+m_-}{m_+ + m_-} \mathbf{u} \times \dot{\mathbf{u}}. \quad (11)$$

Setting $m_-\mathbf{u}_+ = m_+\mathbf{u}_-$, we obtain for the dynamically induced moment according to Eq. (1)

$$\mathbf{M} = \mathbf{m}_+ + \mathbf{m}_- = \frac{q}{2} \frac{m_+ - m_-}{m_+ + m_-} \mathbf{u} \times \dot{\mathbf{u}}. \quad (12)$$

Taking $\mathbf{M} = \gamma\mathbf{L}$, we obtain for the gyromagnetic ratio

$$\gamma = \frac{q}{2} \left(\frac{1}{m_-} - \frac{1}{m_+} \right). \quad (13)$$

For nonequal charges, this equation generalizes to

$$\gamma = \frac{m_+}{m_-} \frac{q_+}{m_+ + m_-} - \frac{m_-}{m_+} \frac{q_-}{m_+ + m_-}. \quad (14)$$

Hence, from Eqs. (13) and (14) it becomes apparent that the total gyromagnetic ratio of ion and electron is dominated by the electron mass ($m_i/m_e \sim 10^3-10^5$). Here we need to distinguish between a direct coupling of the electron to the external field $\sim \epsilon_0(\epsilon_{\alpha\beta} - \delta_{\alpha\beta})E_\beta$ as well as an induced motion of the electrons due to the ionic movement. While the former contribution to the total magnetization should vanish with vanishing electric field, the latter should be present as long as the ionic movement persists. More precise analysis will be a topic of a separate publication.

We propose KTO as a prominent candidate for the observation of dynamical multiferroicity. Our findings open up a route for the experimental detection of entangled dynamical orders. They should also motivate further studies of the candidate materials for the realization of the effect.

Acknowledgments. We are grateful to G. Aeppli, U. Aschauer, M. Basini, M. Pancaldi, O. Tjernberg, I. Sochnikov, N. Spaldin, and J. Weissenrieder for useful discussions. We acknowledge support from VILLUM FONDEN via the Centre of Excellence for Dirac Materials (Grant No. 11744), the European Research Council under the European Union Seventh Framework ERS-2018-SYG 810451 HERO, and the Knut and Alice Wallenberg Foundation KAW 2018.0104. V.J. acknowledges the support of the Swedish Research Council (VR 2019-04735), and J.-X.Z. was supported by the Los Alamos National Laboratory LDRD Program. S.B. acknowledges support from the Swedish Research Council (VR 2018-04611). The computational resources were provided by the Swedish National Infrastructure for Computing (SNIC) via the High Performance Computing Centre North (HPC2N) and the Uppsala Multidisciplinary Centre for Advanced Computational Science (UPPMAX).

-
- [1] D. M. Juraschek, M. Fechner, A. V. Balatsky, and N. A. Spaldin, Dynamical multiferroicity, *Phys. Rev. Mater.* **1**, 014401 (2017).
- [2] H. Katsura, N. Nagaosa, and A. V. Balatsky, Spin Current and Magnetoelectric effect in Noncollinear Magnets, *Phys. Rev. Lett.* **95**, 057205 (2005).
- [3] J. D. Jackson, *Classical Electrodynamics* (Wiley, New York, 1999).
- [4] D. E. Khmel'Nitskiĭ and V. L. Shneerson, Phase transitions of the displacement type in crystals at very low temperatures, *Sov. J. Exp. Theor. Phys.* **37**, 164 (1973).
- [5] S. E. Rowley, L. J. Spalek, R. P. Smith, M. P. M. Dean, M. Itoh, J. F. Scott, G. G. Lonzarich, and S. S. Saxena, Ferroelectric quantum criticality, *Nat. Phys.* **10**, 367 (2014).
- [6] P. Chandra, G. G. Lonzarich, S. E. Rowley, and J. F. Scott, Prospects and applications near ferroelectric quantum phase transitions: a key issues review, *Rep. Prog. Phys.* **80**, 112502 (2017).
- [7] R. Rousev and A. J. Millis, Theory of the quantum paraelectric-ferroelectric transition, *Phys. Rev. B* **67**, 014105 (2003).
- [8] J. M. Edge, Y. Kedem, U. Aschauer, N. A. Spaldin, and A. V. Balatsky, Quantum Critical Origin of the Superconducting Dome in SrTiO₃, *Phys. Rev. Lett.* **115**, 247002 (2015).
- [9] C. W. Rischau, X. Lin, C. Grams, D. Finck, S. Harms, J. Engelmayer, T. Lorenz, Y. Gallais, B. Fauque, J. Hemberger, and B. Kamran, A ferroelectric quantum phase transition inside the superconducting dome of Sr_{1-x}Ca_xTiO_{3-δ}, *Nat. Phys.* **13**, 643 (2017).
- [10] A. Narayan, A. Cano, A. V. Balatsky, and N. A. Spaldin, Multiferroic quantum criticality, *Nat. Mater.* **18**, 223 (2018).
- [11] J. R. Arce-Gamboa and G. G. Guzman-Verri, Quantum ferroelectric instabilities in superconducting SrTiO₃, *Phys. Rev. Mater.* **2**, 104804 (2018).
- [12] K. Dunnett, J.-X. Zhu, N. A. Spaldin, V. Juričić, and A. V. Balatsky, Dynamic Multiferroicity of a Ferroelectric Quantum Critical Point, *Phys. Rev. Lett.* **122**, 057208 (2019).
- [13] A. Khaetskii, V. Juričić, and A. V. Balatsky, Thermal magnetic fluctuations of a ferroelectric quantum critical point, *J. Phys.: Condens. Matter* **33**, 04LT01 (2021).
- [14] D. M. Juraschek, M. Fechner, and N. A. Spaldin, Ultrafast Structure Switching Through Nonlinear Phononics, *Phys. Rev. Lett.* **118**, 054101 (2017).
- [15] M. E. Lines and A. M. Glass, *Principles and Applications of Ferroelectrics and Related Materials* (Oxford University Press, Oxford, 2001).

- [16] I. S. Golovina, S. P. Kolesnik, V. P. Bryksa, V. V. Strelchuk, I. B. Yanchuk, I. N. Geifman, S. Khainakov, S. V. Svechnikov, and A. N. Morozovska, Defect driven ferroelectricity and magnetism in nanocrystalline KTaO_3 , *Physica B* **407**, 614 (2012).
- [17] R. L. Prater, L. L. Chase, and L. A. Boatner, Raman scattering studies of the impurity-induced ferroelectric phase transition in KTaO_3 : Nb, *Phys. Rev. B* **23**, 221 (1981).
- [18] M. Tyunina, J. Narkilahti, M. Plekh, R. Oja, R. M. Nieminen, A. Dejneka, and V. Trepakov, Evidence for Strain-Induced Ferroelectric order in Epitaxial Thin-Film KTaO_3 , *Phys. Rev. Lett.* **104**, 227601 (2010).
- [19] E. A. Zhurova, Y. Ivanov, V. Zavodnik, and V. Tsirelson, Electron density and atomic displacements in KTaO_3 , *Acta Crystallogr., Sect. B* **56**, 594 (2000).
- [20] A. Togo and I. Tanaka, First principles phonon calculations in materials science, *Scr. Mater.* **108**, 1 (2015).
- [21] G. Kresse and J. Furthmüller, Efficient iterative schemes for *ab initio* total-energy calculations using a plane-wave basis set, *Phys. Rev. B* **54**, 11169 (1996).
- [22] J. P. Perdew, K. Burke, and M. Ernzerhof, Generalized Gradient Approximation Made Simple, *Phys. Rev. Lett.* **77**, 3865 (1996).
- [23] R. M. Geilhufe and W. Hergert, GTPack: A mathematica group theory package for application in solid-state physics and photonics, *Front. Phys.* **6**, 86 (2018).
- [24] W. Hergert and R. M. Geilhufe, *Group Theory in Solid State Physics and Photonics: Problem Solving with Mathematica* (Wiley-VCH, Weinheim, Germany, 2018).
- [25] E. Farhi, A. K. Tagantsev, R. Currat, B. Hehlen, E. Courtens, and L. A. Boatner, Low energy phonon spectrum and its parameterization in pure KTaO_3 below 80 K, *Eur. Phys. J. B* **15**, 615 (2000).
- [26] P. Ghosez, J.-P. Michenaud, and X. Gonze, Dynamical atomic charges: The case of ABO_3 compounds, *Phys. Rev. B* **58**, 6224 (1998).
- [27] K. Persson, Materials Data on KTaO_3 (SG:221) by Materials Project (2014), accessed, March 3rd 2021.
- [28] A. Cartella, T. F. Nova, M. Fechner, R. Merlin, and A. Cavalleri, Parametric amplification of optical phonons, *Proc. Natl. Acad. Sci. USA* **115**, 12148 (2018).
- [29] P. Salèn, M. Basini, S. Bonetti, J. Hebling, M. Krasilnikov, A. Y. Nikitin, G. Shamuilov, Z. Tibai, V. Zhaunerchyk, and V. Goryashko, Matter manipulation with extreme terahertz light: Progress in the enabling THz technology, *Phys. Rep.* **836**, 1 (2019), matter manipulation with extreme terahertz light: Progress in the enabling THz technology.
- [30] Y. T. Rebane, Faraday effect produced in the residual ray region by the magnetic moment of an optical phonon in an ionic crystal, *Zh. Eksp. Teor. Fiz.* **84**, 2323 (1983).